Penerbit UTHM

IJIE

Journal homepage: http://penerbit.uthm.edu.my/ojs/index.php/ijie
ISSN : 2229-838X e-ISSN : 2600-7916

The International Journal of Integrated Engineering

Catalytic Steam Reforming of Toluene for Hydrogen Production over Nickel-Cobalt Supported Activated Carbon

Hamdya Sabrina Mohidin Yahya, Nor Aishah Saidina Amin*

Chemical Reaction Engineering Group (CREG), School of Chemical & Energy Engineering, Faculty of Engineering, Universiti Teknologi Malaysia (UTM), Johor Bahru, 81310, MALAYSIA.

*Corresponding's author

DOI: https://doi.org/10.30880/ijie.2019.11.07.027
Received 16 July 2019; Accepted 20 October 2019; Available online 15 November 2019

Abstract: Tar formation during biomass gasification is the main obstacle in the sustainable hydrogen (H_2) production, which increases the processing cost due to clogging of pipes and engines as well as reducing the desired product efficiency. In this present study, catalytic performance of Ni and/or Co supported on modified-palm kernel shell-derived activated carbon (AC) catalysts in steam reforming of toluene (tar model compound) for H_2 production was investigated. Experiments were performed to investigate the effect of several factors on toluene conversion ($X_{toluene}$) and H_2 yield (Y_{H2}), including surface pretreatment using nitric acid to AC support and metal loading content of Ni and/or Co. The synthesized catalysts were characterized using FTIR, BET, XRD, TGA and FESEM-EDX. The 10%Ni-10%Co/ACN catalyst exhibited the highest $X_{toluene}$ and Y_{H2} with 70% and 69%, respectively, attributed by its improved coke-resistance capability during reaction. This is contributed from the formation of Ni-Co solid solution alloys and homogenous metal distribution due to the increment of surface area, microporous structure and surface functional group after pretreatment. Bimetallic Ni-Co supported on modified-AC catalyst has high potential as low-cost biomass-derived catalyst in tar removal for hydrogen production.

Keywords: Activated carbon, steam reforming, toluene, hydrogen

1. Introduction

Global energy supply is almost entirely dependent on fossil fuels such as oil, coal and natural gas [1]. Thus, utilization of non-renewable resources has led to a significant increase of greenhouse gas emission affecting the environment due to climate change. Therefore, reduction of global warming impact has driven the attention towards utilizing renewable source of energy, including biomass [2]. Synthesis gas (syngas), a mixture of primarily carbon monoxide (CO) and hydrogen (H_2) has been seen as a promising energy source to replace conventional fossil fuel-based energy. Syngas can also be utilized as an alternative to natural gas fuel for power or H_2 production. Compared to fossil fuel, biomass has significant advantages such as abundantly available, inexhaustibility, renewability, carbon-neutrality and low sulfur content. The syngas can also be used further as a feedstock for the production of hydrocarbon fuels via the Fischer-Tropsch synthesis (FTS) process. However, biomass-based syngas contains high concentration of tars byproducts, which represent a mixture of several aromatic compounds, that prevents the syngas from direct use and requires an effective tar removal approach. It is essential to remove tar content prior to syngas utilization because the inevitable tars-byproduct causes clogging of lines and heat exchangers as well as catalyst deactivation due to coke formation [3]. Tar formation poses as the greatest hurdles of successful implementation of biomass gasification technologies in a commercial scale. Hence, the removal of tar in biomass gasification is highly desirable.

Catalytic steam reforming (SR) of tar is one of the most promising technique because of its high conversion efficiency for hydrogen production [4]. Additionally, catalytic SR of tars is able to increase syngas production where it

*Corresponding author: noraishah@cheme.utm.my

is usually insufficient for FTS (requires about H_2/CO =2) and other syngas conversion. However, due to complexity of tar compositions, different model molecules representatives of tar have been used in previous studies such as toluene, benzene, phenol, and naphthalene. Nickel (Ni)-based catalysts are widely used as SR catalyst because of its high activity, low-cost and easy regeneration [5], but tends to suffer from catalyst deactivation during SR of toluene (SRT) caused by coke deposition and metal sintering. Thus, modification of Ni-based catalyst towards promoting higher catalytic performance in SR with more coke-resistant and stable catalyst is still a challenge at present. One of the successful modification techniques in improving the catalytic performances of Ni-based catalyst in steam reforming for hydrogen production is the addition of second metals such as cobalt (Co). Ebshish and coworkers reported that the addition of Co in Ni/γ-Al_2O_3 catalyst exhibited higher catalytic performance with better activity and hydrogen selectivity as compared to Ni/γ-Al_2O_3 promoted with Na, Fe and Cu [6]. Bimetallic catalyst has been proven to increase the catalytic efficiency due to synergistic combination of both metals improving stability and resistance from deactivation [7, 8]. Ni and Co metal catalysts are cost effective and makes it as promising candidates for SRT Several studies have reported that bimetallic Ni-Co catalyst produced higher conversion in SRT and other tar model compounds for H_2 production with high stability in SR reaction [9-12]. In fact, Co catalyst registered much higher activity than Ni catalysts and has been extensively used in SR of oxygenates (methanol and ethanol) [13]. However, supported metal catalysts possess more advantages in many respects than unsupported metal catalysts [5].

Catalyst support plays an important role for supported metal catalyst to provide a structural framework and stabilizes the active metal species as well as the enhancement of mechanically robustness of the catalyst [14]. In some cases, the support itself provides the new active sites to the system especially those that comprises of both acidic and basic functional groups. The main objective in metal supported catalyst preparation for SRT is to obtain the catalyst in a high dispersion of the catalytically active metal on the surface of support while promoting carbon removal or suppressing its formation. Recent interest in utilizing activated carbon-supported metals catalysts in steam reforming of tar has emerged [15-17]. Activated carbon (AC) exhibits unique properties when it is used as a catalyst support, such as high surface area, stable in both acidic and basic media, as well as possibility of tuning both its textural surface characteristic and surface chemical properties [18, 19]. Catalytic reactivity of AC-based catalyst is driven by the high surface area properties as well as the oxygen-containing functional groups on its surface. Other than that, metal dispersion and metal-carbon interaction also affect catalytic reactivity in SR reaction.

The dispersion of active metal particles is highly influenced by the preparation of support material. Oxidizing pretreatment of AC support using nitric acid, hydrogen peroxide and sulfuric acid is able to improve the surface properties as well as to increase the surface oxygen functional groups. Improving the dispersion of active metal particles on AC support material generally increases the catalytic activity [17]. Catalytic activity test using pretreated-AC supported metal catalyst exhibited higher conversion efficiency as compared to untreated AC catalyst [16, 20, 21]. Thus, the objective of this study is to evaluate the catalytic performance of nickel and/or cobalt supported nitric acid-pretreated AC in SRT for hydrogen production. Critical evaluation of catalyst physicochemical properties on activity and stability is expected to elucidate the effectiveness of the synthesized catalyst in SRT and tar removal.

2. Materials and Methodology

Raw palm kernel shell-derived activated carbon (AC) (1-5 mm) was purchased from Multi Filter Sdn Bhd (Malaysia). AC was washed with distilled water to remove impurities and oven-dried at 110 °C overnight. Nitric acid (65%, Mërck) was used to modify AC support prior metal impregnation step. High purity commercial powder of nickel (II) nitrate hexahydrate ($Ni(NO_3)_2.6H_2O$) (98%, Mërck) and cobalt (II) nitrate hexahydrate ($Co(NO_3)_2.6H_2O$) (98%, Sigma-Aldrich) were used as metal oxide precursor to impregnate AC support. Metal nitrates and analytical toluene (98%, QRëc) were used as received without further treatment.

2.1 Catalyst Preparation

2.1.1 Pretreatment of AC Support

Palm kernel shell-derived AC (AC) was used as catalyst support after surface modification. First, raw AC granules was grinded and sieved to obtain particles with diameter <100 μm. Nitric acid (HNO_3) was used as an oxidizing agent for AC surface pretreatment in a liquid phase treatment. In this process, AC particles were dispersed in boiling deionized water and heated for 2h. AC was filtered and washed for several times to remove ash. The filtered and washed-out AC was re-dispersed in 400 ml 10 wt.% HNO_3 aqueous solution and refluxed at 80 ^oC for 5h. Finally, HNO_3-pretreated AC (ACN) sample was filtered and thoroughly washed with distilled water until pH=7. It was then dried in the oven for 12h at 110 ^oC.

2.1.2 Metal-supported Catalysts Preparation

The dried AC pretreated by HNO_3 as described earlier was used as catalyst support. The synthesis of monometallic and bimetallic Ni and/or Co supported on ACN catalysts was carried out via wet impregnation using metal nitrate hexahydrate of Ni and/or Co as metal precursor. In this process, 2.5g of ACN support was impregnated with 10 wt.%

metal loading of $Ni(NO_3)_2.6H_2O$ and/or $Co(NO_3)_2.6H_2O$ solution. The ratio between ACN and metal nitrate solution is maintained at 2.5g:100 ml. The suspension was under magnetic stirring for 5h at 60ºC. Resultant slurry was further heated to 110ºC to evaporate the solution. Subsequently, the obtained solid was oven-dried overnight at 110ºC and calcined at 500ºC for 4h. The final calcined samples were crushed and stored in a desiccator until further use. The synthesized samples are denoted as 10%Ni-ACN, 10%Co-ACN and 10%Ni-10%Co/ACN, accordingly.

2.2 Catalysts Characterization

Different techniques were employed for catalysts characterization. To determine the influence of HNO_3 pretreated-AC in metal impregnation, Fourier Transform Infrared spectroscopy and multi-point BET-nitrogen (N_2) adsorption-desorption was employed to determine surface oxygen functional group and surface properties, respectively. FTIR spectrums were obtained in the range of 4000-400 cm^{-1} using a Fourier Transform Spectrophotometer with Perkin Elmer Spectrum One instrument (Perkin Elmer, USA). BET surface area analysis was determined through N_2-sorption of BET multi-points analysis using a surface area and porosity analyser (Thermo Scientific Surfer Analyzer, Thermo Fisher Scientific, Italy) via N_2 adsorption-desorption isotherm collected at 77K. Subsequently, powder X-ray diffraction analysis of catalysts were conducted to identify crystalline phases of Ni and Co present in the catalysts. XRD experiments were performed using D5000 Siemens instrument recorded over an angular range 2θ from 20◦ to 90◦ with a scanning rate of 1.2◦ min^{-1} via Ni-filtered Cu-kα radiation (40 keV, 40 mA). Thermal behaviour of catalyst samples was also recorded by thermogravimetric analysis (TGA) and differential thermal analysis (DTA) using TGA 8000 system with Pyris Diamond TG/DTA apparatus from Perkin Elmer instruments (Perkin Elmer, USA) under N_2 environment with a ramp rate of 10 ◦C min to 900 ◦C. Field Emission Scanning Electron Microscopy equipped with Energy Dispersive X-ray spectrometer (FESEM-EDX) using Hitachi SU8020 integrated with beam of X-Max^N by Oxford instrument optics (Hitachi High-Technologies Corporation, Japan) was employed to investigate catalysts surface morphology and distribution of Ni and/or Co metal on the ACN support.

2.3 Catalytic Activity in Steam Reforming of Toluene

The experimental setup consists of a preheater, furnace, stainless steel fixed bed reactor, high pressure liquid HPLC pump, syringe pump, a circular cooling unit, a condenser and a gas chromatography (GC) equipped with flame ionization detector (FID) and thermal conductivity detector (TCD) (Fig. 1). The mixed water-toluene liquid feed at a total feed flow rate of 8.25 ml/min was flowed into the preheater using high-performance metering pump (HPLC) and syringe pump. It was then completely vaporized through the preheater set at 200 ºC. N_2 was used as carrier gas at controlled rate of 15 ml/min which was maintained by mass flow controller (Alicat Scientific, USA). The N_2-vaporised feed mixture were flowed into a 13 mm diameter stainless-steel fixed bed reactor loaded with catalyst (0.3g) placed in between ceramic wools to ensure fixed position of catalyst. SRT reaction was conducted at steam-to-carbon (S/C) ratio and temperature of 5 and 700 ºC, respectively. Effect of stainless-steel reactor and ceramic wool was considered negligible in calculating the catalytic activity and selectivity. The gaseous product was cooled to 10 ºC using a condenser and analyzed online using Agilent GC 6890N equipped with FID (detection of H_2, CO and CO_2), TCD (detection of hydrocarbon) and capillary columns (Agilent, 60 m × 0.32 mm ID;HP-Plot Q, 40 m × 0.53 mm ID, 40 µm; and Molsieve, 30 m × 0.530 mm ID, 25 µm). The total flow rate of produced gas was measured using digital flow meter.

Equations (1) to (4) were used to calculate toluene conversion ($X_{toluene}$), yield of hydrogen (Y_{H2}) and carbon-containing product (Y_i). Y_{H2} was expressed as percentage of actual H_2 produced per maximum mole of stoichiometric H_2 produced, assuming 1 mole of toluene produced 18 moles of H_2. F^{out} and F^{in} are output and input molar flow rates, respectively.

$$X_{toluene}(\%) = \frac{F_{CO}^{out} + F_{CO_2}^{out} + F_{CH_4}^{out}}{7 \times F_{toluene}^{in}} \times 100 \quad (1)$$

$$Y_{H_2}(\%) = \frac{F_{H_2}^{out}}{18 \times F_{Toluene}^{in}} \times 100 \quad (2)$$

$$Y_i(\%) = \frac{\#C \times F_i^{out}}{7 \times F_{toluene}^{in}} \times 100 \quad (3)$$

Molar flow rates of H_2, CO, CO_2, CH_4 (products) and toluene (reactant) at outlet and inlet are specified in mol/h unit and denoted as $F_{H_2}^{out}$, F_{CO}^{out}, $F_{CO_2}^{out}$, $F_{CH_4}^{out}$ and $F_{toluene}^{in}$, accordingly. Product selectivity is the molar percentage of products obtained, excluding unconverted toluene, water and N_2 (carrier gas).

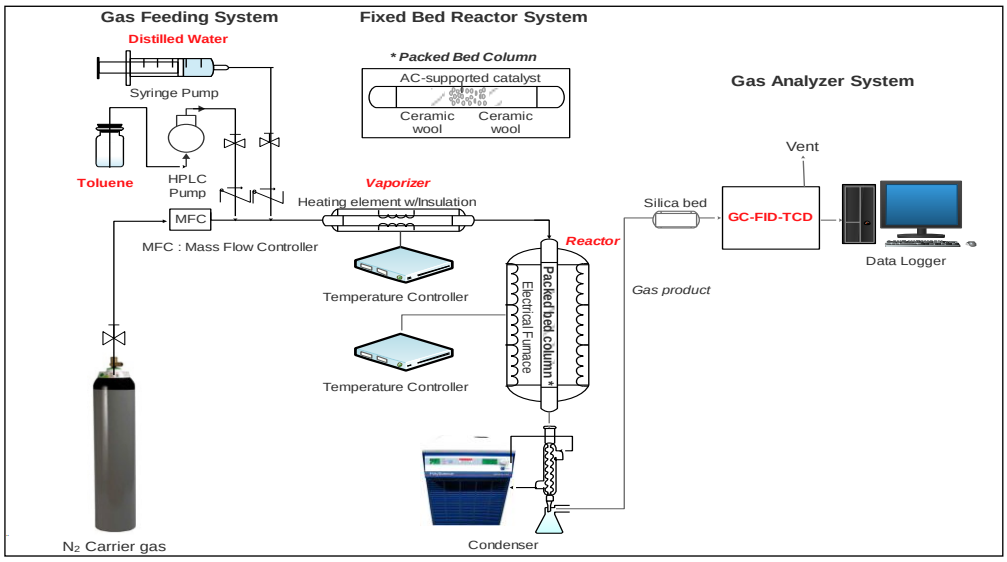

Fig. 1 Schematic layout of experimental setup of catalytic SRT for hydrogen production.

3. Results and Discussions

3.1 Catalyst Characterization

The surface oxygenated functional groups (SOFG) present in the untreated AC, ACN and the synthesized catalyst samples (Ni/ACN, Co/ACN and NiCo/ACN) are determined by FTIR analysis. The resultant FTIR spectra (Fig. 2a) exhibit a broad band at 3440 cm^{-1} attributed by hydroxyl (OH^-) groups associated to moisture present in the five catalyst samples [22]. Other prominent peaks are observed in 400-1700 cm^{-1} region. The band peak at 1717 cm^{-1} are attributed by C=O (carboxyl and carboxylate group) which has increased upon HNO_3 pretreatment [23]. The presence of these functional groups will increase the hydrophilicity properties of the carbon materials and assists the adsorption of metal ions onto the surface of AC support more homogeneously [20]. However, decreasing peak at ~1425 cm^{-1} of ACN catalyst compared to AC indicates C-O of quinonic group reduced after pretreatment suggesting the corrosive nature of nitric acid had caused the removal of this group [24, 25]. Furthermore, the possible presence of Ni- and/or Co-ACN complex [23] with band peak of Co-O and Ni-O at ~669 cm^{-1}, 568 cm^{-1} and ~466 cm^{-1}, respectively, which are not present in AC and ACN samples indicate the tensile vibration of Ni-O and Co-O bands [26]. These results confirm the successful incorporation of Ni^{2+} and/or Co^{2+} cations onto the surface of ACN supported catalysts.

Based on N_2 adsorption-desorption isotherm analysis (Fig. 2b), textural properties of synthesized catalysts such as BET surface area (S_{BET}), micropore surface area (S_{micro}), pore volume (V_t) and average pore diameter are summarized in Table 1. The isotherms for AC, ACN and Ni-Co/ACN catalysts depict hybrid characteristic of Type I and IV according to the IUPAC classification, indicating micropores and mesoporous material [27]. The uptake for ACN sample higher than AC infers that amount of micropores increased after the HNO_3 pretreatment. The surface pretreated ACN gives significant increment of S_{BET}, S_{micro} and V_t amount compared to AC. The addition of 10 wt.% Ni and Co loading gives smaller S_{BET}, S_{micro} and V_t compared to AC and ACN samples. It could be attributed to the successful metal impregnation and partial pore filling of Ni-Co/ACN [23]. This can be confirmed further by FESEM-EDX through metal distribution mapping of Ni-Co/ACN catalyst.

Table 1 Surface properties of the prepared catalysts.

Catalysts	BET surface area, S_{BET} (m^2 g^{-1})	Micropore surface area, S_{micro} (m^2g^{-1})	Pore volume, V_t (cm^3 g^{-1})	Average pore diameter (nm)
Untreated AC	684.29	632.86	0.32	2.12
ACN	850.03	775.61	0.50	1.87
10%Ni-10%Co/ACN	462.66	397.77	0.28	2.40

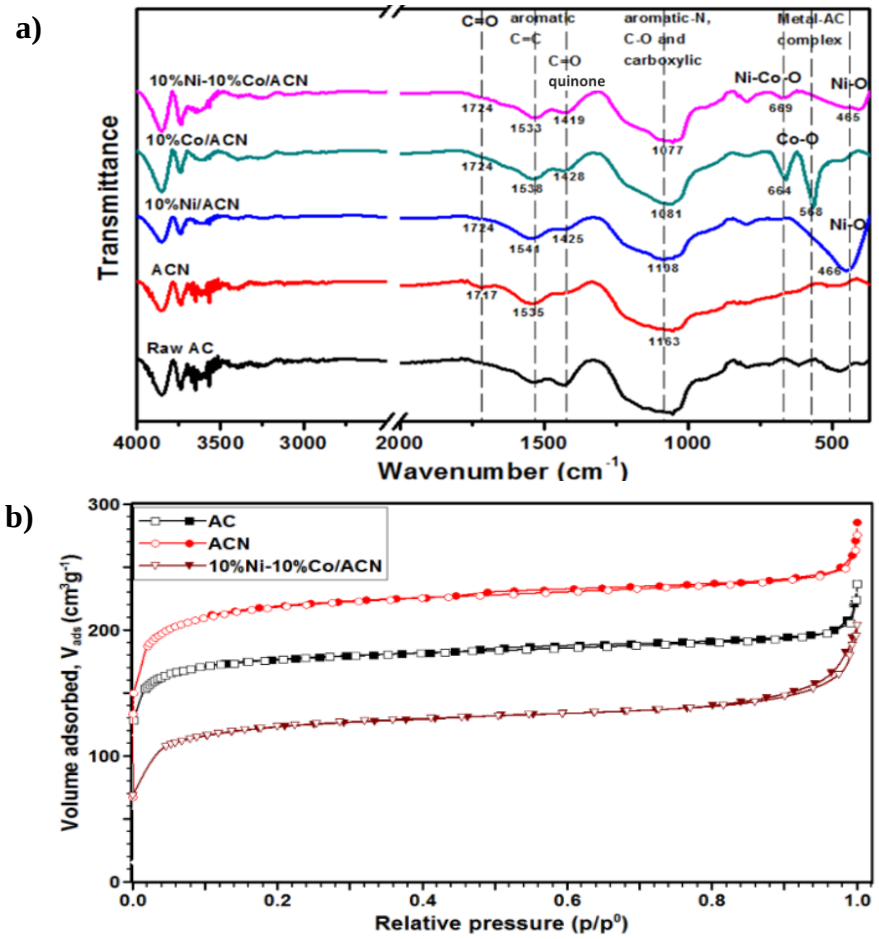

Fig. 2 (a) FTIR spectrums of AC, ACN, Ni/ACN, Ni/ACN and Ni-Co/ACN catalysts; and (b) N_2-adsorption desorption isotherm of AC, ACN and Ni-Co/ACN catalysts.

Powder X-ray Diffraction (XRD) analysis was employed to determine crystallite phase and structure of Ni-Co supported on ACN catalyst. Fig. 3a shows the effect of XRD pattern of raw AC and bimetallic Ni-Co supported ACN catalysts. AC sample displays broad diffraction peaks at 2θ angles of 25.3º (002) and 43.62º (101), which can be assigned as amorphous and graphene or graphite carbon (ICDD PDF-2# 01-041-1487). Saleh and Danmaliki also found similar XRD patterns of AC without pretreatment [28]. Slight decrease of these peaks upon impregnation were observed for 10%Ni-10%Co/ACN. Similar findings, reported by Cui *et. Al.*, claimed the crystallinity of AC decreased slightly upon metal impregnation [29]. Bimetallic Ni-Co supported ACN depict diffraction patterns of nickel oxide and/or cobalt oxide at 2θ angles of 31.18º, 36.75º, 42.83º, 43.45º, 59.10º, 62.23º, 64.50º, 74.60º and 78.43º which is consistent with library XRD of NiO (ICDD PDF-2# 01-078-4374), CoO (ICDD PDF-2# 01-070-2855) and Co_3O_4 (ICDD PDF-2# 03-065-3103). This confirms the active phases of NiO, CoO and Co_3O_4 are present in Ni-Co supported ACN catalyst as listed in Table 2 corresponding to the facets of each compound [30, 31]. Furthermore, the presence of NiO and CoO or Co_3O_4 phase in bimetallic supported catalysts also affects the diffraction peaks where the diffraction peaks are seen to be shifted slightly to lower value of 2θ for carbon [28, 32]. These may be contributed by the formation of interacted species between Ni and Co with ACN support [31]. These findings are in agreement with the data reported in the ICDD PDF-2 card and those reported in previous studies.

Carbon deposition is one of the major limitations in SR reaction. This is because it has tendency to block active metal sites leading catalyst deactivation. Thermogravimetric analysis (TGA) and differential thermogravimetric analysis (DTA) were employed to provides insights of the amount and nature of deposited carbon over spent catalysts of 10%Ni/ACN, 10%Co/ACN and 10%Ni-10%Co/ACN after 5h in SRT reaction from 20 to 900 ºC, as shown in Fig. 3b. Initial decomposition at temperature between 20-80 ºC is associated with the release of moisture and physisorbed water from the surface of catalysts. The weight loss reached up to 10% for both 10%Ni/ACN and 10%Co/ACN, whereas 10%Ni-10%Co/ACN only have slight weight loss of moisture in this region. Subsequently, all catalysts conferred profound weight losses starting at 530 ºC until 550 ºC attributed by the total oxidation of carbon to CO_2. High temperature of oxidation indicates the decomposition of carbon nanotube is around 450-550 ºC [33, 34]. The amount of coke formation was observed to be decreasing for 10%Co/ACN, 10%Ni/ACN and 10%Ni-10%Co/ACN with 30 wt.%, 15 wt.% and 8 wt.%, respectively. The weight decrease occurred above 550 ºC for all catalysts owing to the formation

of graphite carbon, as observed by Quitete *et al* [35]. The final weight loss of catalysts occurred at 900 ºC was established in the following order 10%Ni-10%Co/ACN < 10% Ni/ACN < 10%Co/ACN with 20%, 24% and 45%, respectively. This suggested the relative resistance of carbon formation on the Ni-Co/ACN catalyst. The synergetic combination of active metal Ni-Co alloys onto support had successfully eliminated significant amount of inert or graphitic carbon.

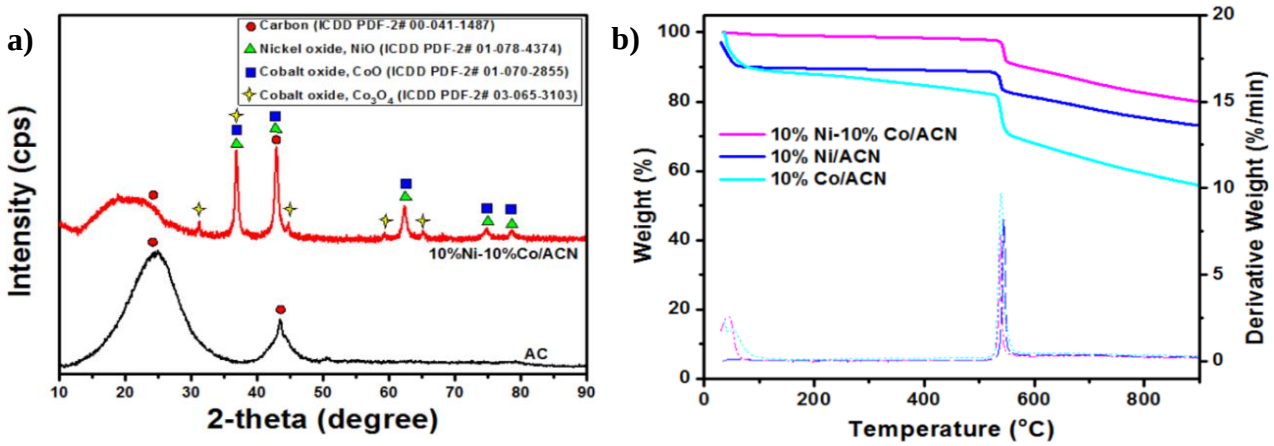

Fig. 3 (a) XRD patterns of AC and 10%Ni-10%Co/ACN; and (b) TGA/DTA profile of spent 10% Ni/ACN, 10% Co/ACN and 10% Ni-10% Co/ACN catalysts after 5h in SRT.

Table 2 XRD analysis of the 10%Ni-10%Co/ACN catalyst.

	2θ (degree)	hkl indices	ICDD (PDF-2)
AC	25.30	002	01-075-2078
	43.62	101	
NiO	36.9	101	01-078-4374
	42.93	012	
	62.43	110	
	75.04	113	
	78.91	202	
CoO	36.9	111	01-070-2855
	42.93	200	
	62.43	331	
	75.04	220	
	78.91	311	
Co_3O_4	36.9	311	03-065-3103
	64.8	400	

FESEM-EDX analysis was used to investigate the morphology and active metal distribution on the surface of catalyst support. The morphology of untreated AC, ACN and the active metal Ni-Co loaded on ACN catalysts with different magnification scales were obtained and presented in Fig. 4. The ACN (Fig. 4b) shows increase of pore formation after the surface treatment with HNO_3 compared to AC (Fig. 4a) as confirmed by the BET analysis. The 10%Ni-10%Co/ACN catalyst (Fig. 4c-f) revealed that the metal particles in the catalyst samples with irregular shapes. Partial pore blockage could have occurred due to the deposition of active metals on the surface and into the pores of the support [23]. The distribution of Ni and Co metal on the support are demonstrated with cyan and purple dots as depicted in Fig. 4g. Both metal-impregnated catalysts displayed uniform distribution of Ni and Co on the surface of AC support inferring the effectiveness of nitric acid pretreatment method for AC support prior to metal impregnation leading to uniform metal dispersion on the support. However, it is also observed upon 25000-40000x magnification that micropores are still partially vacant. Table 3 indicates the weight percent of Ni and Co on ACN support of the Ni-Co/ACN which almost similar to the desired metal loading.

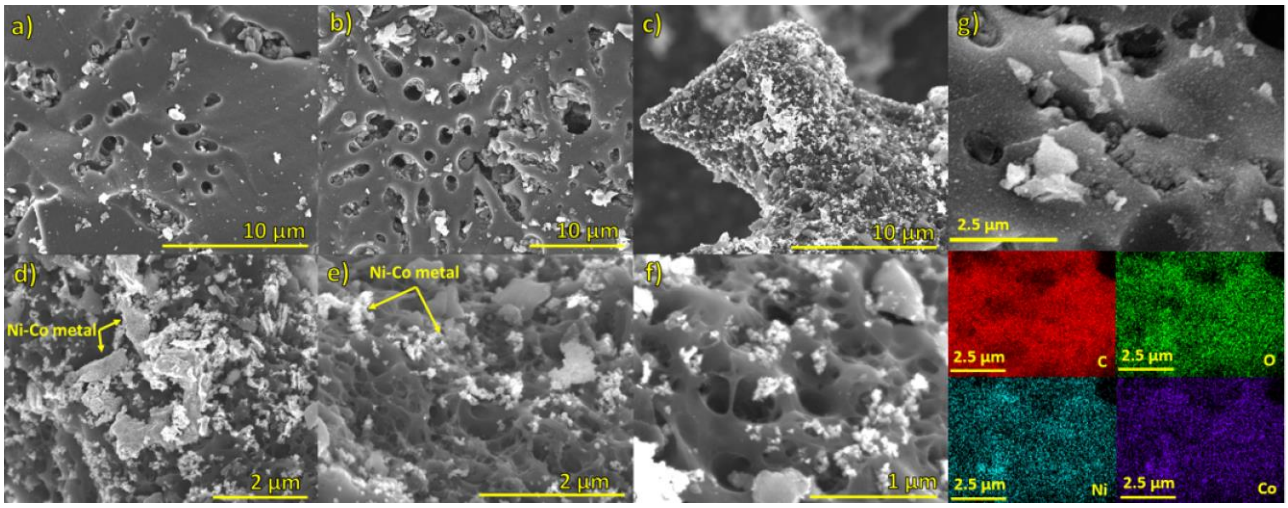

Fig. 4 FESEM images for (a) untreated AC at 5000x; (b) ACN at 5000x; (c) 10%Ni-10%Co/ACN at 5000x; (d) 10%Ni-10%Co/ACN at 15000x; (e) 10%Ni-10%Co/ACN at 25000x; (f) 10%Ni-10%Co/ACN at 40000x; and (g) EDX mapping for 10%Ni-10%Co/ACN catalyst.

Table 3 The loading of Ni and Co on the ACN for 10%Ni-10%Co/ACN catalyst.

Catalyst	10%Ni-10%Co/ACN			
Elements	O	C	Ni	Co
Weight %	63.8	15.6	10.9	9.8

3.2 Catalytic Activity in Steam Reforming of Toluene

Catalytic activities of homogenous (no catalyst), untreated AC, Ni/ACN, Co/ACN and Ni-Co/ACN were evaluated in SRT for hydrogen production during 5h of testing time. The hydrogen yield (Y_{H2}), carbon-containing product yield (Y_i) and toluene conversion ($X_{toluene}$) into gaseous products were evaluated for all catalysts. As depicted in Fig. 5a and 5b, increasing $X_{toluene}$ and Y_{H2} were observed in SRT with the addition of 10%Co, 10%Ni and 10%Ni-10%Co. The catalyst with 10%Ni-10%Co exhibited the best catalytic performance: the $X_{toluene}$ and Y_{H2} was obtained at 70% and 69%, respectively. Excellent performance of bimetallic 10%Ni-10%Co/ACN catalyst is attributed by the synergistic combination of Ni-Co and high metal dispersion on the AC-modified catalyst support, as proven by the XRD pattern and FESEM-EDX images. High dispersion of active metal particles is contributed by the enhancement of SOFG based on the FTIR spectra which then promotes the homogenous active metal distribution. Furthermore, higher coke-resistant property is registered through the TGA evaluation with the lowest amount of coke deposited on used of 10%Ni-10%Co/ACN catalyst compared to the other catalysts. It has been reported that bimetallic Ni-Co catalysts performed well in SR reactions of coal tar [36], toluene [37], and phenol [10]. In addition, Y_{CO2} for 10%Ni/ACN is significantly lower as compared to 10%Ni-10%Co/ACN at 19% and 42%, respectively. This may be due to lower active metal sites on 10%Ni/ACN compared to 10%Ni-10%Co/ACN. Fig. 5c and 5d depict the catalytic activities of Y_{H2} and $X_{toluene}$, respectively, as a function of time on stream for the catalysts. Increasing trend of Y_{H2} and $X_{toluene}$ are observed for 10%Ni-10%Co/ACN. Meanwhile, Y_{H2} over 10%Ni/ACN reduced significantly after 3h of reaction. This phenomenon is expected as Ni catalyst commonly undergoes significant deactivation in SRT owing to carbon deposition [38, 39], whereas, low catalytic activities or almost no activities are observed for homogenous, AC and 10%Co/ACN. The deactivation behavior of Co catalyst in CO_2 reforming of toluene is also reported previously by Bao *et al* due to the sintering effect of metallic Co particles, which depend on the amount of Co loading amount [40]. However, the addition of Co as a metal promoter in bimetallic supported catalyst has shown good results in SR reactions due to the strong interaction between Ni and Co alloy that enhances the carbon resistant property [37].

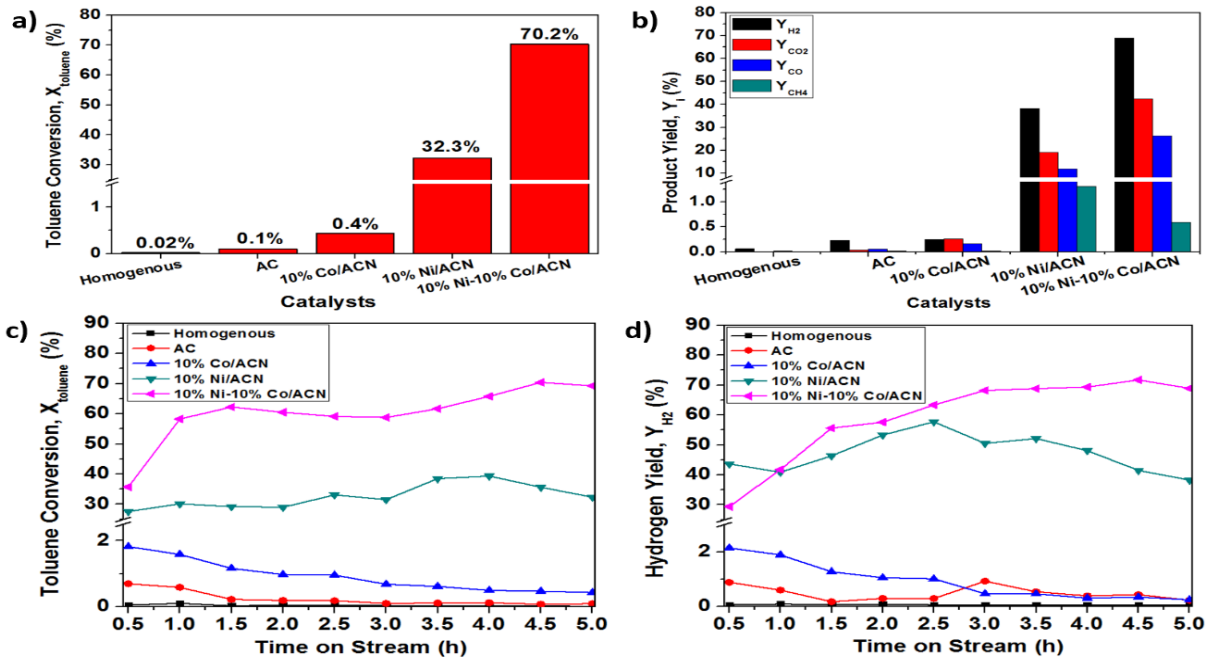

Fig. 5 Catalytic SRT for homogenous, AC, 10%Co/ACN, 10%Ni/ ACN and 10%Ni-10%Co/ACN after 5h of (a) toluene conversion; (b) product yield; (c) toluene conversion over time on stream; and (d) hydrogen yield over time on stream.

The main reactions involved in this study are the reaction of SRT (Equation 4-5) and water gas shift (WGS) (Equation 6) [38]. The mechanism initiated by the adsorption of the toluene onto the surface of metal particles followed by toluene dealkylation to benzene and methane (Equation 7). Methane either reacts immediately with water producing H_2 and CO (Equation 8), or further dehydrogenates to CH_x species and carbon. Higher formation of CO_2 compared to CO over 10%Ni-10%Co/ACN is mainly attributed to the enhanced WGS side reaction that accompanied the SRT reaction. The WGS reactions consume CO and produces more H_2 and CO_2, leading to the higher H_2/CO ratio. Formation of carbon may be the main contributor of the loss of catalytic activity in SRT owing to the Boudouard reaction (Equation 9). The amount of carbon deposited on the spent catalyst obtained from TGA results reveal that higher carbon formation leads to the degradation of catalytic activity. Castro *et al* reported that increased amount of carbon formation was contributed by the increased acid sites density of catalysts [41, 42]. The main route of carbon deposition on the surface of catalyst could be attributed to oligomerization of toluene on the acidic sites of catalyst support [43].

Steam reforming of toluene :

$$C_7H_8 + 14H_2O \rightarrow 7CO_2 + 18H_2 \quad \Delta H_{700^\circ C} = 680kJ/mol \tag{3}$$

$$C_7H_8 + 7H_2O \rightarrow 7CO + 11H_2 \quad \Delta H_{700^\circ C} = 925kJ/mol \tag{4}$$

Water gas shift :

$$CO + H_2O \rightleftharpoons CO_2 + H_2 \quad \Delta H_{700^\circ C} = -35kJ/mol \tag{5}$$

Hydrodealkylation:

$$C_7H_8 + H_2 \rightarrow C_6H_6 + CH_4 \tag{7}$$

Methane steam reforming:

$$CH_4 + H_2O \rightarrow CO + 3H_2 \tag{8}$$

Boudouard reaction:

$$C + CO_2 \rightleftharpoons 2CO \tag{9}$$

4. Conclusion

The modified AC-supported Ni and/or Co catalyst were prepared and tested in steam reforming of toluene as biomass tar model compound. The optimum preparation conditions for the AC-supported catalyst are 10 wt.% of Ni and Co loading supported on the HNO_3-preteated AC as catalyst support. The 10%Ni-10%Co/ACN catalyst composition exhibits the best catalytic performance in SRT with the highest catalytic activity at 72% toluene conversion ($X_{toluene}$) and 62% hydrogen yield (Y_{H2}) obtained after 5h. Surface modification of AC support using nitric acid has enhanced the impregnation of active bimetals to highly disperse Ni and Co onto the AC surface. The high surface area, microporous structure, enhancement of SOFG and synergistic combination of Ni-Co alloy formation on

the surface of ACN support serve as important roles in the improvement of the catalytic activity. These enhancement leads to the coke-resistance capability of the 10%Ni-10%Co/ACN catalyst where the deposited coke amount reduces significantly compared to the other catalysts. Thus, the high performance of 10%Ni10%Co/ACN catalyst demonstrates its potential as a biomass-based catalyst in tar removal for hydrogen production.

Acknowledgement

This research is supported by Tier 1 Research University Grant Scheme of Universiti Teknologi Malaysia (17H09). Also, the assistance from University Laboratory Management Unit (UPMU) and Analytical Lab in School of Chemical and Energy Engineering, Faculty of Engineering, Universiti Teknologi Malaysia are highly acknowledged.

References

[1] British Petroleum (2017). BP Energy Outlook 2017 Edition, 1-104.
[2] Baykara S. Z. (2018). Hydrogen: A brief overview on its sources, production and environmental impact. International Journal of Hydrogen Energy, 43, 10605-10614.
[3] Rios M. L. V., González A. M., Lora E. E. S., Olmo O. A. A. d. (2018). Reduction of tar generated during biomass gasification: A review. Biomass and Bioenergy, 108, 345–370.
[4] Guan G., Kaewpanha M., Hao X., Abudula A. (2016). Catalytic steam reforming of biomass tar: Prospects and challenges. Renewable and Sustainable Energy Reviews, 58, 450-461.
[5] Li D., Tamura M., Nakagawa Y., Tomishige K. (2015). Metal catalysts for steam reforming of tar derived from the gasification of lignocellulosic biomass. Bioresource Technology, 178, 53-64.
[6] Ebshish A., Yaakob Z., Narayanan B., Bshish A., Daud W. R. W. (2011). The activity of Ni-based catalysts on steam reforming of glycerol for hydrogen production. International Journal of Integrated Engineering, 3, 5-8.
[7] Bizkarra K., Bermudez J. M., Arcelus-Arrillaga P., Barrio V. L., Cambra J. F., Millan M. (2018). Nickel based monometallic and bimetallic catalysts for synthetic and real bio-oil steam reforming. International Journal of Hydrogen Energy, 43, 11706-11718.
[8] Wang L., Li D., Koike M., Watanabe H., Xu Y., Nakagawa Y., Tomishige K. (2013). Catalytic performance and characterization of Ni–Co catalysts for the steam reforming of biomass tar to synthesis gas. Fuel, 112, 654-661.
[9] Gai C., Zhang F., Yang T., Liu Z., Jiao W., Peng N., Liu T., Lang Q., Xia Y. (2018). Hydrochar supported bimetallic Ni–Fe nanocatalysts with tailored composition, size and shape for improved biomass steam reforming performance. Green Chemistry, 20, 2788-2800.
[10] Nabgan W., Tuan Abdullah T. A., Mat R., Nabgan B., Triwahyono S., Ripin A. (2016). Hydrogen production from catalytic steam reforming of phenol with bimetallic nickel-cobalt catalyst on various supports. Applied Catalysis A: General, 527, 161-170.
[11] Heo D. H., Lee R., Hwang J. H., Sohn J. M. (2016). The effect of addition of Ca, K and Mn over Ni-based catalyst on steam reforming of toluene as model tar compound. Catalysis Today, 265, 95-102.
[12] Hu S., He L., Wang Y., Su S., Jiang L., Chen Q., Liu Q., Chi H., Xiang J., Sun L. (2016). Effects of oxygen species from Fe addition on promoting steam reforming of toluene over Fe–Ni/Al_2O_3 catalysts. International Journal of Hydrogen Energy, 41, 17967-17975.
[13] Xing R., Dagle V. L., Flake M., Kovarik L., Albrecht K. O., Deshmane C., Dagle R. A. (2016). Steam reforming of fast pyrolysis-derived aqueous phase oxygenates over Co, Ni, and Rh metals supported on $MgAl_2O_4$. Catalysis Today, 269, 166-174.
[14] He L., Hu S., Jiang L., Liao G., Chen X., Han H., Xiao L., Ren Q., Wang Y., Su S., Xiang J. (2018). Carbon nanotubes formation and its influence on steam reforming of toluene over Ni/Al_2O_3 catalysts: Roles of catalyst supports. Fuel Processing Technology, 176, 7-14.
[15] Augusto B. L., Ribeiro M. C., Aires F. J. C. S., da Silva V. T., Noronha F. B. (2018). Hydrogen production by the steam reforming of ethanol over cobalt catalysts supported on different carbon nanostructures. Catalysis Today.
[16] Veiga S., Bussi J. (2017). Steam reforming of crude glycerol over nickel supported on activated carbon. Energy Conversion and Management, 141, 79-84.
[17] Liu X., Yang X., Liu C., Chen P., Yue X., Zhang S. (2016). Low-temperature catalytic steam reforming of toluene over activated carbon supported nickel catalysts. Journal of the Taiwan Institute of Chemical Engineers, 65, 233-241.
[18] Ng C. A., Wong L. Y., Bashir M. J. K., Ng S. L. (2018). Development of hybrid polymeric polyerthersulfone (PES) membrane incorporated with powdered activated carbon (PAC) for palm oil mill effluent (POME) treatment. International Journal of Integrated Engineering, 10, 137-141.
[19] Daud Z., Ahmad B., Awang H., Abubakar M. H., Ridzuan M. B., Tajarudin H. A. (2018). Removal of COD using delonix regia pods activated carbon adsorbent for natural rubber wastewater treatment. International Journal of Integrated Engineering, 10, 77-83.
[20] Shen C., Zhou W., Yu H., Du L. (2018). Ni nanoparticles supported on carbon as efficient catalysts for steam reforming of toluene (model tar). Chinese Journal of Chemical Engineering, 26, 322-329.

[21] Bhandari P. N., Kumar A., Bellmer D. D., Huhnke R. L. (2014). Synthesis and evaluation of biochar-derived catalysts for removal of toluene (model tar) from biomass-generated producer gas. Renewable Energy, 66, 346-353.
[22] Zhang Y., Lei H., Yang Z., Duan D., Villota E., Ruan R. (2018). From glucose-based carbohydrates to phenol-rich bio-oils integrated with syngas production via catalytic pyrolysis over an activated carbon catalyst. Green Chemistry, 20, 3346-3358.
[23] Yadav B. R., Garg A. (2016). Catalytic oxidation of pulping effluent by activated carbon-supported heterogeneous catalysts. Environmental Technology, 37, 1018-1025.
[24] Jahromi F. G., Ghahreman A. (2019). Effect of surface modification with different acids on the functional groups of AF5 catalyst and its catalytic effect on the atmospheric leaching of enargite. Colloids and Interfaces, 3, 45-61.
[25] ShamsiJazeyi H., Kaghazchi T. (2010). Investigation of nitric acid treatment of activated carbon for enhanced aqueous mercury removal. Journal of Industrial and Engineering Chemistry, 16, 852-858.
[26] Chen Y., Lu W., Guo Y., Zhu Y., Lu H., Song Y. (2018). Synthesis, characterization and photocatalytic activity of nanocrystalline first transition-metal (Ti, Mn, Co, Ni and Zn) oxisde nanofibers by electrospinning. Applied Sciences, 9, 8-24.
[27] Sing K. S. W. (1985). Reporting physisorption data for gas/solid systems with special reference to the determination of surface area and porosity (Recommendations 1984). Pure and Applied Chemistry, 57, 603–619.
[28] Saleh T. A., Danmaliki G. I. (2016). Influence of acidic and basic treatments of activated carbon derived from waste rubber tires on adsorptive desulfurization of thiophenes. Journal of the Taiwan Institute of Chemical Engineers, 60, 460-468.
[29] Cui B., Zhang J., Liu S., Liu X., Xiang W., Liu L., Xin H., Lefler M. J., Licht S. (2017). Electrochemical synthesis of ammonia directly from N_2 and water over iron-based catalysts supported on activated carbon. Green Chemistry, 19, 298-304.
[30] Guan Q., Chen S., Chen Y., Gu J., Li B., Miao R., Chen Q., Ning P. (2017). High performance noble-metal-free NiCo/AC bimetal for gasification in supercritical water. International Journal of Hydrogen Energy, 42, 6511-6518.
[31] Chen X., Carabineiro S. A. C., Bastos S. S. T., Tavares P. B., Órfão J. J. M., Pereira M. F. R., Figueiredo J. L. (2013). Exotemplated copper, cobalt, iron, lanthanum and nickel oxides for catalytic oxidation of ethyl acetate. Journal of Environmental Chemical Engineering, 1, 795-804.
[32] Lankitsi J. Malobela J. H., Willem G. Augustyn, Leskey M. Cele (2014). Nickel−cobalt on carbonaceous supports for the selective catalytic hydrogenation of cinnamaldehyde. Industrial & Engineering Chemistry Research, 53, 13910-13919.
[33] Jabbour K., Massiani P., Davidson A., Casale S., El Hassan N. (2017). Ordered mesoporous "one-pot" synthesized Ni-Mg(Ca)-Al_2O_3 as effective and remarkably stable catalysts for combined steam and dry reforming of methane (CSDRM). Applied Catalysis B: Environmental, 201, 527-542.
[34] Yang W., Liu H., Li Y., Wu H., He D. (2016). CO_2 reforming of methane to syngas over highly-stable Ni/SBA-15 catalysts prepared by P123-assisted method. International Journal of Hydrogen Energy, 41, 1513-1523.
[35] Quitete C. P. B., Manfro R. L., Souza M. M. V. M. (2017). Perovskite-based catalysts for tar removal by steam reforming: Effect of the presence of hydrogen sulfide. International Journal of Hydrogen Energy, 42, 9873-9880.
[36] Gao N., Han Y., Quan C. (2018). Study on steam reforming of coal tar over NiCo/ceramic foam catalyst for hydrogen production: Effect of Ni/Co ratio. International Journal of Hydrogen Energy, 43, 22170-22186.
[37] Li Z., Li M., Ashok J., Kawi S. (2019). NiCo@NiCo phyllosilicate@CeO_2 hollow core shell catalysts for steam reforming of toluene as biomass tar model compound. Energy Conversion and Management, 180, 822-830.
[38] Cao J.-P., Ren J., Zhao X.-Y., Wei X.-Y., Takarada T. (2018). Effect of atmosphere on carbon deposition of Ni/Al_2O_3 and Ni-loaded on lignite char during reforming of toluene as a biomass tar model compound. Fuel, 217, 515-521.
[39] Zhang Z., Liu L., Shen B., Wu C. (2018). Preparation, modification and development of Ni-based catalysts for catalytic reforming of tar produced from biomass gasification. Renewable and Sustainable Energy Reviews, 94, 1086-1109.
[40] Bao X., Kong M., Lu W., Fei J., Zheng X. (2014). Performance of Co/MgO catalyst for CO_2 reforming of toluene as a model compound of tar derived from biomass gasification. Journal of Energy Chemistry, 23, 795-800.
[41] de Castro T. P., Silveira E. B., Rabelo-Neto R. C., Borges L. E. P., Noronha F. B. (2018). Study of the performance of Pt/Al_2O_3 and Pt/CeO_2/Al_2O_3 catalysts for steam reforming of toluene, methane and mixtures. Catalysis Today, 299, 251-262.
[42] de Castro T. P., Peguin R. P. S., Neto R. C. R., Borges L. E. P., Noronha F. B. (2015). Steam reforming of toluene over Pt/$Ce_xZr_{1-x}O_2$/Al_2O_3 catalysts. Topics in Catalysis, 59, 292-302.
[43] Silveira E. B., Rabelo-Neto R. C., Noronha F. B. (2017). Steam reforming of toluene, methane and mixtures over Ni/ZrO_2 catalysts. Catalysis Today, 289, 289-301.